scientific reports

OPEN

Computational drug design for neurosyphilis disease by targeting *Phosphoglycerate Kinase* in *Treponema pallidum* with enhanced binding affinity and reduced toxicity

Muhammad Naveed[1✉], Shumaila Ibrahim[1], Tariq Aziz[2✉], Muhammad Asim[1], Muhammad Nouman Majeed[1], Ayaz Ali Khan[3], Rania Ali El Hadi Mohamed[4], Maher S. Alwethaynani[5], Fakhria A. Al-Joufi[6] & Deema Fallatah[7]

Neurosyphilis, a severe neurological complication of syphilitic infection caused by the gram-negative spirochete *Treponema pallidum* poses significant challenges in treatment due to its irregular physiology and lack of efficacy in present therapeutic strategies. Here, we report a new approach to developing drug treatment that targets the enzyme *phosphoglycerate kinase* (PGK), an essential component of the *T. pallidum* glycolytic pathway. Therefore, a ligand was designed involving common neuroprotectant elements reported from literature by a computational drug design method, to increase their binding energy with lower toxicity. The calculated binding affinity of the designed ligand with PGK was analyzed by molecular docking to be − 116.68 kcal/mol. Also, interaction analysis predicted that there are 5 hydrophobic bonds and 3 hydrogen bonds present between the docked complex. Afterward, *in-silico* ADMET studies were conducted for the designed ligand that determined a strong pharmacological profile with good absorption, zero violation of Lipinski's rule, and non-toxic properties. DFT analysis further optimized the ligand with a HOMO/LOMO gap value of 0.01421 kcal/mol indicating higher reactivity and enhanced electronic interactions, improving ligand efficiency. Moreover, pharmacophore modeling confirmed the reactive nature of the ligand. Furthermore, MD simulations showed stability in the overall structure. The output shows that our optimized ligand has statistically better binding affinity than the currently used drug penicillin, with improved pharmacokinetic profiles. This work demonstrates the importance of ligand design for the discovery of new drugs to treat neurosyphilis.

Keywords Neurosyphilis, *T. pallidum*, *Phosphoglycerate kinase*, Computational drug design, Neuroprotectant elements

Neurosyphilis, a significant problem arising from untreated syphilis, constitutes a major health concern, especially due to infection caused by a spirochete bacterium *Treponema pallidum*. *Treponema pallidum* subspecies pallidum, recognized as the etiological agent responsible for syphilis, spreads throughout the body within hours to days after the initial inoculation[1]. The initial of the central nervous system (CNS) is believed

[1]Department of Biotechnology, Faculty of Science and Technology, University of Central Punjab, Lahore 54590, Pakistan. [2]Laboratory of Animal Health Food Hygiene and Quality, University of Ioannina, Arta, Greece. [3]Department of Biotechnology, University of Malakand, Chakdara, Dir Lower, Pakistan. [4]Department of Biology, College of Science, Princess Nourah bint Abdulrahman University, P.O.Box 84428, 11671 Riyadh, Saudi Arabia. [5]Department of Clinical Laboratory Sciences, College of Applied Medical Sciences, Shaqra University, Alquwayiyah, Riyadh, Saudi Arabia. [6]Department of Pharmacology, College of Pharmacy, Jouf University, 72341 Aljouf, Saudi Arabia. [7]Department of Medical Laboratory Sciences, College of Applied Medical Sciences, Prince Sattam Bin Abdulaziz University, 11942 Al-Kharj, Saudi Arabia. ✉email: Naveed.quadian@gmail.com; iwockd@gmail.com

to become apparent in a significant proportion of individuals infected with syphilis. Consequently, it is not unexpected that neurological manifestations related to syphilis may arise at any phase of the infection[2]. While syphilis initially presents as a sexually transmitted infection, if not treated, the bacterium has the potential to disseminate throughout the organism and ultimately infiltrate the central nervous system (CNS), leading to the condition known as neurosyphilis. This pathological state may arise at any phase of syphilis, although it is predominantly linked to the advanced stages of the infection[3]. Neurosyphilis can present in an array of manifestations, ranging from asymptomatic cases to severe neurological damages, comprising meningitis, dementia, ataxia, and even symptoms reminiscent of a cerebrovascular accident. The affliction signifies one of the serious complications associated with *T. pallidum* infection, underscoring the bacterium's ability to impact various organ systems, notably the brain and spinal cord[1]. In the year 2012, a total of 18 million cases of syphilis were documented across the globe, among which 350,000 instances resulted in damaging pregnancy outcomes[4]. The prevalence of this condition continues to accelerate, primarily due to the proliferation of at-risk populations, which encompasses men who engage in sexual activities and individuals living with HIV (PLWH)[5]. The prevalence of neurosyphilis among PLWH is approximately twice that observed in the immunocompetent demographic. Despite the relatively low incidence of syphilis among women in the United States, there was a notable increase of 30.0% during the period from 2018 to 2019; concerning congenital syphilis, the incidence has similarly demonstrated an upward trajectory since the year 2013. In the context of China, the cases of syphilis rose from 0.9 to 34.49 per million between 1990 and 2017, ranking in second position after viral hepatitis and tuberculosis among infectious diseases[6].

In the pre-antibiotic age, patients frequently underwent a series of lumbar lesions to evaluate the therapeutic efficacy of arsenicals, as part of efforts to treat the infection and slow down the advancement of central nervous system (CNS) pathology[7]. Arsenicals and all other treatments utilized before the advent of penicillin were ineffective in eliminating *T. pallidum*. Following the extensive implementation of penicillin treatment after World War II, the incidence of syphilis within the USA experienced a significant decline over several decades. Nonetheless, the achievements of penicillin treatment, and various medical dimensions of syphilis, particularly neurosyphilis, continue to pose challenges in the control of this condition[8]. The determination to conduct a lumbar lesion, the analysis of cerebrospinal fluid (CSF) results, the establishment of strong treatment criteria for neurosyphilis, the formulation of standard treatment protocols, and the strategy for monitoring patients with neurosyphilis remain imbued with ambiguity. Furthermore, developing drug resistance to antibiotics is a growing concern[9].

One of the promising approaches for combating Neurosyphilis is using computational methods for designing drugs against key enzymes of *T. pallidum*. The causative agent of syphilis, *Treponema pallidum*, is a spirochete bacterium that is highly invasive and has an especially unique ability to escape the immune system and cause polymorphic infections[10]. This pathogen is quite reliant on the nutrients provided by the host due to the deficiency of many biosynthetic pathways within it[11]. Phosphoglycerate kinase (PGK) is considered one of the important enzymes for many organisms. It is involved in the metabolic function, as it catalyzes the transfer of a phosphate group between two intermediates in carbohydrate metabolism. It is considered a crucial enzyme in the glycolytic pathway of *T. pallidum*, facilitating the reversible transfer of a phosphate moiety from 1,3-bisphosphoglycerate to ADP, thereby generating ATP and 3-phosphoglycerate. As this enzyme is important for the energy metabolism of *T. pallidum*, the inhibition of this enzyme will ultimately inhibit the carbohydrate metabolism and ATP generation ultimately leading to bacterial growth inhibition has been raised as a key drug target for bacterial pathogens, encompassing *T. pallidum*[12]. The inhibition of PGK activity could upset the energy production mechanisms of the bacterium, ultimately leading to growth inhibition of *T. pallidum*. Furthermore, the conserved nature of PGK's active site presents a viable chance for designing high-affinity therapeutics with reduced side effects, making it an appropriate candidate for targeted therapeutic strategies in treating neurosyphilis[13]. Currently, there are no PGK-targeted drugs approved for treating neurosyphilis, but several studies are exploring glycolytic enzyme inhibitors for bacterial infections[14]. There are no clinical trials of PGK inhibitors have been conducted. However small inhibitors of enzymes such as carbonic anhydrases are being studied in clinical trials that catalyze the breakdown of glucose within other pathogens such as *Mycobacterium Tuberculosis* or *Plasmodium falciparum*[15]. A search of clinical trial databases indicates that while specific PGK inhibitors are under evaluation for cancer[15], none have progressed to human trials specifically for *T. pallidum* infections.

In recent years, the field of computational drug design has fundamentally transformed the discipline of medicinal chemistry, allowing researchers to determine potential inhibitors of target proteins through computational approaches. Computational techniques, including molecular docking, molecular dynamics (MD) simulations, and free energy calculations, have been used in modern drugs and the identification of flavor compounds from plant resources as well. These methodologies allow for the identification of molecular modifications that can enhance sweetness while minimizing bitterness, thereby improving the overall palatability of Stevioside. Molecular docking enables the prediction of binding affinities between taste-modified compounds and their respective receptor targets, offering a structure-based approach to rational compound design[16]. Computational biology helps in the identification of drug compounds from a large compound of the library within a short period as in previous studies the identification of cyclin-dependent kinase 2 for the treatment of different types of cancers[17,18]. Through Insilco approaches it has become possible to find out the inhibitors against MDR bacteria and viruses as well. Computational methodologies facilitate the discovery of inhibitors against viruses characterized by enhanced binding affinity and specificity by targeting specific viral proteins as done by the study[17,18]. These methodologies prominently reduce the time and cost linked with conventional drug design approaches[19]. Moreover, computational strategies yield profound insights into the interaction mechanisms between pharmacological candidates and target proteins at the atomic level, thereby advancing the optimization of binding affinity, selectivity, and pharmacokinetic attributes. By using these tools, it becomes

feasible to design innovative drug candidates that not only demonstrate strong binding affinity for PGK but also exhibit less toxicity and enhanced drug-likeness, thereby ensuring their clinical effectiveness and safety. The key objective of this study is to contribute to the advancement of efficacious and safe treatments for neurosyphilis that overcome the limitations of current antibiotics.

Methodology

Retrieval of tertiary structure of protein
The 3D structure of the protein Phosphoglycerate Kinase of the bacterium *Treponema pallidum* was retrieved from the alpha fold database (https://alphafold.ebi.ac.uk/)[20] with alpha fold protein ID of B2S3D0, an artificial intelligence application developed by DeepMind which is employed for the prediction of three-dimensional protein structures utilizing a deep learning framework. Alpha Fold is experiencing accelerated research advancements across nearly all biological fields. The 3D structure of PGK was further predicted by using Robetta (https://robetta.bakerlab.org/) and I teaser server (https://zhanggroup.org/I-TASSER/). Based on the comparison validation of the predicted model, the final 3D model of the receptor was selected and used for further analysis[21].

Structure validation
To validate a protein's 3D structure, Ramachandran plots were generated using the PROCHECK server (https://saves.mbi.ucla.edu)[22]. THE ERRAT server was employed to evaluate the quality score of the developed protein structure. The 3D structure model conformation was yielded as input to the server[23].

Binding pockets prediction
The Prank Web server (https://prankweb.cz/), built on machine learning, was used to predict the active sites of proteins[24]. An enzyme or protein possesses a distinct region referred to as a binding site, which facilitates its interaction with specific molecules and the execution of biochemical reactions. The predicted binding pocket on the receptor PGK by the prankweb server was further validated using the BIOVIA Discovery Studio Visualizer[25].

Phylogenetic tree construction
The MEGA-X software was utilized for conducting phylogenetic analysis of particular molecular sequences[26], and a tree was built to analyze the evolutionary links of Phosphoglycerate Kinase (PGK) protein among different strains of *Treponema pallidum* and other closely related species. An alignment and evolutionary map of the sequences were constructed from Ten Homologous Phosphoglycerate Kinase (PGK) sequences.

De Novo ligand sketching
An online computational tool Marvin Sketch (https://marvinjs-demo.chemaxon.com/latest/demo.html) was utilized for the designing of the de Novo ligand[27]. Marvin Sketch represents a Java-based application designed for the graphical representation of chemical structures, facilitating the creation and modification of molecular entities across a range of file formats[28]. Moreover, chemdoodle was used for the generation of the IUPAC name of the de novo-designed ligand[29].

Retrieval of compounds
The reported drug compounds against phosphoglycerate kinase (PGK) in *Treponema pallidum* were identified through a comprehensive literature review. The retrieved inhibitors were then cross-checked and obtained from the PubChem database (https://pubchem.ncbi.nlm.nih.gov/)[30]. The retrieved compounds were further converted into pdb format to prepare them for molecular docking.

Virtual screening by PyRx
Virtual screening was conducted using PyRx to evaluate the binding affinity of reported inhibitors with phosphoglycerate kinase (PGK). Ligand structures were retrieved from PubChem. The Auto Dock Vina module in PyRx was used for molecular docking analysis. The receptor was converted into a macromolecule the format was shifted to pdbqt and the ligands were optimized and converted into auto dock vina format pdbqt[31]. The docking grid was set over the active site of PGK protein with centers of X:0.8302, Y:2.6642, Z:63.8847 and having dimensions X:79.45, Y:63.88 and Z:25. The docking was proceeded and binding affinities were recorded.

Molecular docking analysis
Afterward, the free docking analysis was performed by using the Hdock server (http://hdock.phys.hust.edu.cn/). The HDOCK server works by accepting amino acid sequences as input and using a hybrid docking approach that incorporates experimental data, such as protein–protein binding sites and small-angle X-ray scattering, during docking and post-docking phases[58].

Interaction analysis
The molecular interaction was analyzed using PLIP[32] and BIOVIA Discovery Studio Visualizer[33]. Discovery Studio analyzed the 2D interactions between receptor and protein. Whereas, PLIP (https://plip-tool.biotec.tu-dresden.de/plip-web/plip/index) was used to determine the interacting amino acid residues with the ligand[34].

Pharmacophore characterization
The web-based platform PharmIT (http://pharmit.csb.pitt.edu/) was employed for pharmacophore-based virtual screening[35]. In the context of Pharmacophore design, the molecules included in the test cohort were assigned cluster ID 1, whereas the remaining molecules were categorized within the training set, each possessing distinct

cluster IDs. The ligand collection was subjected to clustering based on their three-dimensional pharmacophore attributes, while all other parameters were maintained at their default settings[36].

ADMET analysis

To evaluate the behavior of the drug with body mechanism SwissADME (http://www.swissadme.ch/) was used. This platform offers predictions regarding critical attributes, including absorption, distribution, metabolism, and excretion in the body. The smiles of drug caudate were provided as input, facilitating the computation of the drug-likeness properties inherent to the compound[37]. Furthermore, the additional toxicity of the designed drug candidate was evaluated by using the Protox II server (https://tox.charite.de/protox3/)[38].

DFT analysis

To evaluate the reactive potential of ligands DFT analysis was conducted. For this analysis, Guass View 5.0 and Gaussian software were utilized, accessible at (https://gaussview.software.informer.com/5.0/). The optimization of the ligand was performed, and DFT analysis was executed employing the RB3LYP method in conjunction with a 6-31G basis set[39]. The electrical energies of both orbitals including the lowest unoccupied molecular orbital (eLumo) and well highest occupied molecular orbital (eHomo) were calculated to elucidate the band energy gap[40].

MD simulation

Molecular dynamics (MD) simulations were executed utilizing the AMBER force fields to accurately model the molecular system[41]. The Apo protein and protein–ligand complex underwent an initial minimization step to alleviate steric clashes, followed by solvation within a periodic box of aqueous molecules and subsequent neutralization through the introduction of counterions. The system was equilibrated through systematic adjustments of temperature and pressure; thereafter, production runs were conducted, yielding trajectory data for the examination of structural properties and interactions over time. The simulations were sustained for a cumulative duration of 100 ns for Apo protein and 300 ns for complex to ensure statistical significance[42].

The MM/GBSA analysis was performed to estimate the binding free energy of the protein–ligand complex obtained from molecular dynamics (MD) simulations. Trajectory files were extracted at specific time intervals to adequately sample the ensemble of conformations representing the dynamic behavior of the system. For each conformation, molecular mechanics energy components, including van der Waals, electrostatic, and torsional energies, were calculated using the molecular mechanics force field. The solvation-free energy was estimated using the Generalized Born (GB) model, incorporating both polar and non-polar contributions to provide a comprehensive evaluation of the system's energetics[43]. Ultimately, the binding free energy was calculated using the formula $\Delta Gbind = \Delta GMM + \Delta Gsolv$, facilitating a thorough assessment of the interactions between the ligand and the target protein[44].

Results

Structure retrieval of the target protein

The 3D structures were retrieved from three tools: I-TASSER, Robetta, and AlphaFold. Among these, the AlphaFold structure was selected ID (B2S3D0). The alignment graph from Alphafold represents the expected positional error (in Angstrom) for residues in the predicted protein structure. High confidence is denoted by dark green, while low confidence is illustrated by lighter green; the diagonal line represents the self-alignment of residues. Given that the alignment graph represents mostly dark green colors along the diagonals, predicting a high confidence score. The retrieved structure is represented in Fig. 1A and the alignment graph in Fig. 1B.

Quality assessment and validation of 3D structure

The selection of the best 3D structure was based on the comparison of different structure prediction tools, considering both Ramachandran (RC) values and ERRAT scores. Although Robetta provided a high-quality score, its RC value was lower, which is a crucial factor for structure validation. In contrast, AlphaFold demonstrated both an excellent RC value (93.8%) and a high ERRAT score (97.27%), making it the most reliable model. Additionally, AlphaFold is a well-established database with experimentally validated structures that are widely accepted in the scientific community. Therefore, the AlphaFold-predicted structure was chosen for further analysis (Table 1).

Moreover, the Ramachandran plot of ProCheck displayed 93.8% residues of protein in the most favorable region by red color, 6.2% residues in the additionally allowed region represented by yellow color and no residues are present in the disallowed region showing a promising model validation for further analysis. Ramachandran plot is depicted in Fig. 2A and ERRAT in 2B below.:

Binding sites prediction

The Prank Web server analyzes the binding pockets in the target protein marked by red color in the 3D structure. At this point, the ligand can completely interact with the target protein. The binding pocket involves 45 residues with a binding score of 49.98. Additionally, DSV validation confirms the presence of a single catalytic site in the PGK structure, reinforcing the accuracy of the predicted binding region (Fig. 3A,B).

Binding site validation with closely related species

The phylogenetic tree presented illustrates the evolutionary relationship of the Phosphoglycerate Kinase (PGK) protein among *Treponema pallidum* strains and closely related species. The inclusion of 10 different sequences confirms the conservation of the PGK binding site across multiple *Treponema* species, supporting the reliability of the predicted binding residues (Fig. 4).

The clustering of *T. pallidum* subtypes indicates a high degree of similarity in PGK sequences, ensuring that the identified binding site remains functionally conserved. Additionally, the validation of these residues
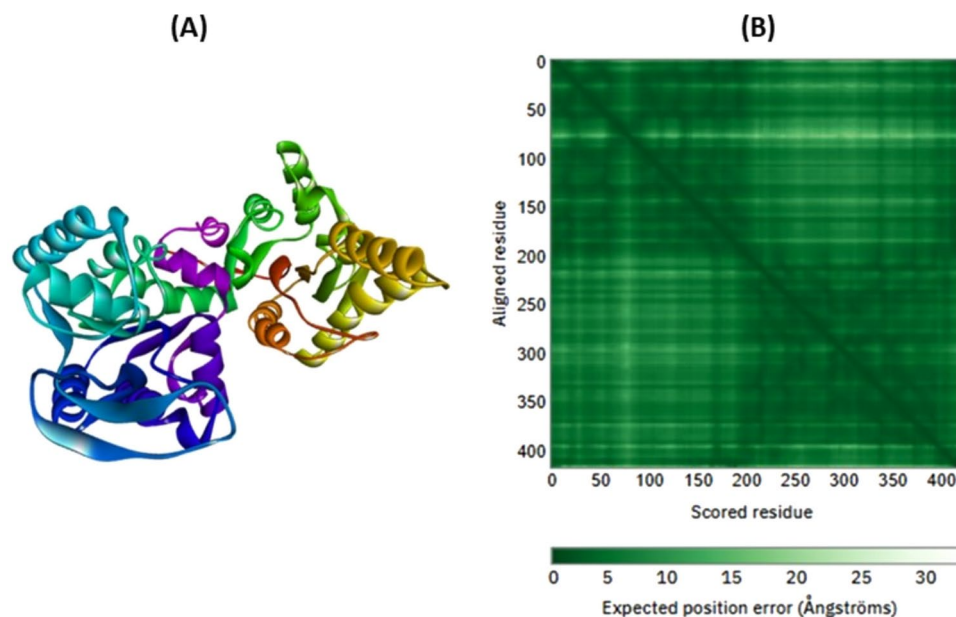
Fig. 1. (**A**) Representation of Protein *Phosphoglycerate Kinase* 3D structure. (**B**) Alignment graph of predicted Protein Phosphoglycerate Kinase 3D structure.

Tools	RC Value (%)	ERRAT Score
I-Tasser	81.7	95.11
Robetta	91.4	98.52
Alphafold	93.8	97.27

Table 1. Comparison of different structure prediction tools based on RC value and ERRAT score.

across evolutionary lineages strengthens their relevance for ligand binding and drug-target interaction studies. This phylogenetic analysis, combined with structural cross-checking using PrankWeb and DSV, confirms the accuracy of the predicted catalytic site.

De-novo ligand design and sketching
Using the MarvinSketch online webserver, a ligand was designed by leveraging the structural characteristics of identified neuroprotective compounds. Two aromatic rings were positioned adjacent to each other. In the first ring, a zinc (Zn) element was connected via a single bond to NH, contributing to the structural stability. Additionally, two hydroxyl groups were introduced at carbon positions 2 and 5 on the same ring, and 1 hydroxyl group and 1 NH_2 and 1 CH_3 on the second ring via a single bond to enhance the stability, binding energy, and solubility of the formed ligand. Integrating conformational favored functional groups enhances ligand binding affinity at the target interface. Hydrogen bonding and optimized hydrophobic interactions stabilize ligands, improving drug efficacy. The introduced hydroxyl, NH2, and CH3 groups enhance stability, solubility, and binding energy, forming three hydrogen bonds and five hydrophobic interactions (Fig. 5). These structural modifications ensure strong protein–ligand stability, crucial for effectively targeting *T. pallidum*. Moreover, the IUPAC name of the designed ligand was generated by drawing the structure using the ChemDoodle 2D server. The generated IUPAC name for the designed ligand was 1,1′-bi(cyclohexane).

Retrieval of the 3D structure of various inhibitors targeting PGK in *Treponema pallidum* treating Neurosyphilis disease
Neurosyphilis is primarily treated with Crystalline Penicillin, but alternatives for penicillin-allergic patients including Adjunctive therapies like Probenecid help manage symptoms. Experimental treatments such as Linezolid, Moxifloxacin, Meropenem, and Fosfomycin are being explored for resistant cases. These approaches aim to inhibit *Treponema pallidum* effectively while addressing drug resistance. The 3D structure of all the inhibitors was retrieved in SDF format from the PubChem database and converted into PDB format from the Discovery Studio visualizer for screening purposes (Table 2).

Comparison of the binding affinity of the 1,1′-bi(cyclohexane) with penicillin
The retrieved inhibitors were docked with the target protein *Phosphoglycerate Kinase* to assess their interactions. The virtual screening analysis, performed using the PyRx software, revealed that 1,1′-bi(cyclohexane) exhibited
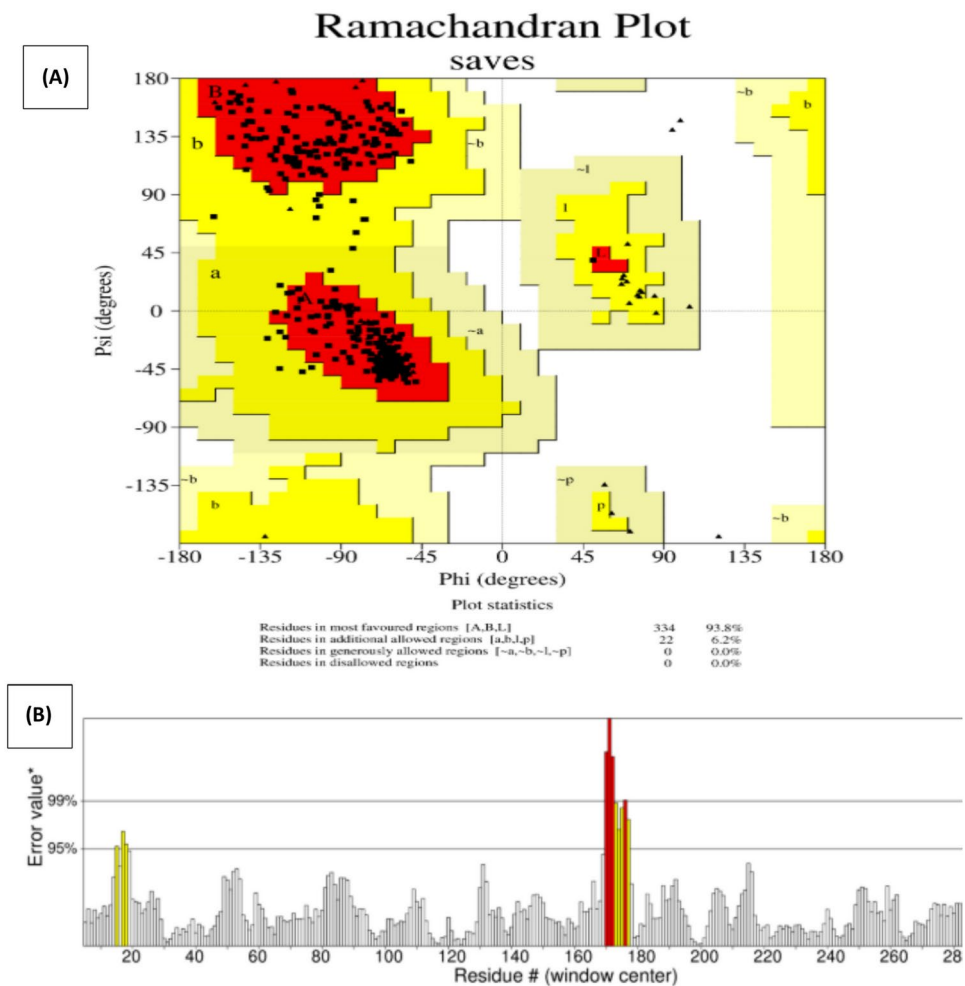
Fig. 2. (**A**) Ramachandran plot showing Phosphoglycerate Kinase protein structure validation, (**B**) ERRAT graph with a score of 97.27% representing the overall quality of protein 3D structure.
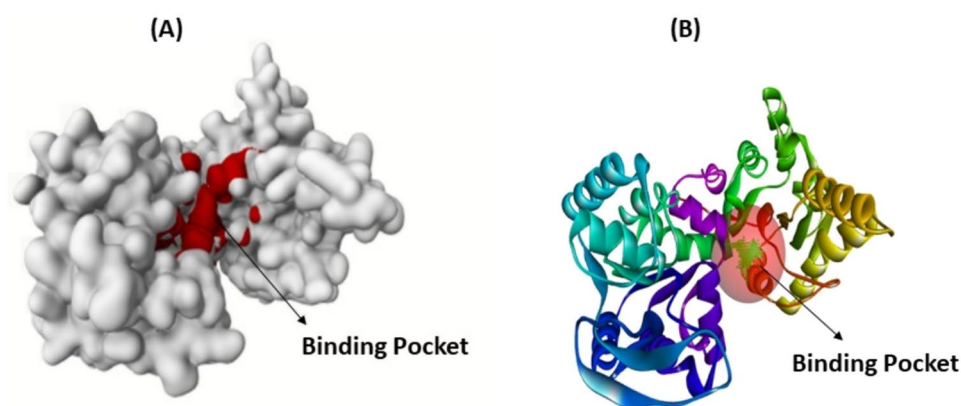

Fig. 3. Binding pocket in protein *Phosphoglycerate Kinase* (**A**) highlighted by red color through Prank web server (**B**) representation through Discovery studio visualizer.

a higher binding energy of −6.5 kcal/mol, compared to others. Afterward, the docking analysis of the designed ligand and penicillin was performed using the HDOCK server to validate the results, which revealed that 1,1′-bi(cyclohexane) exhibited higher binding energy of −116.68 kcal/mol, with a confidence score of 0.3393 and a ligand RMSD of 23.12 Å, compared to penicillin, which showed binding energy of −112.80 kcal/mol, a confidence score of 0.3221, and a ligand RMSD of 29.57 Å. These results indicate that 1,1′-bi(cyclohexane)
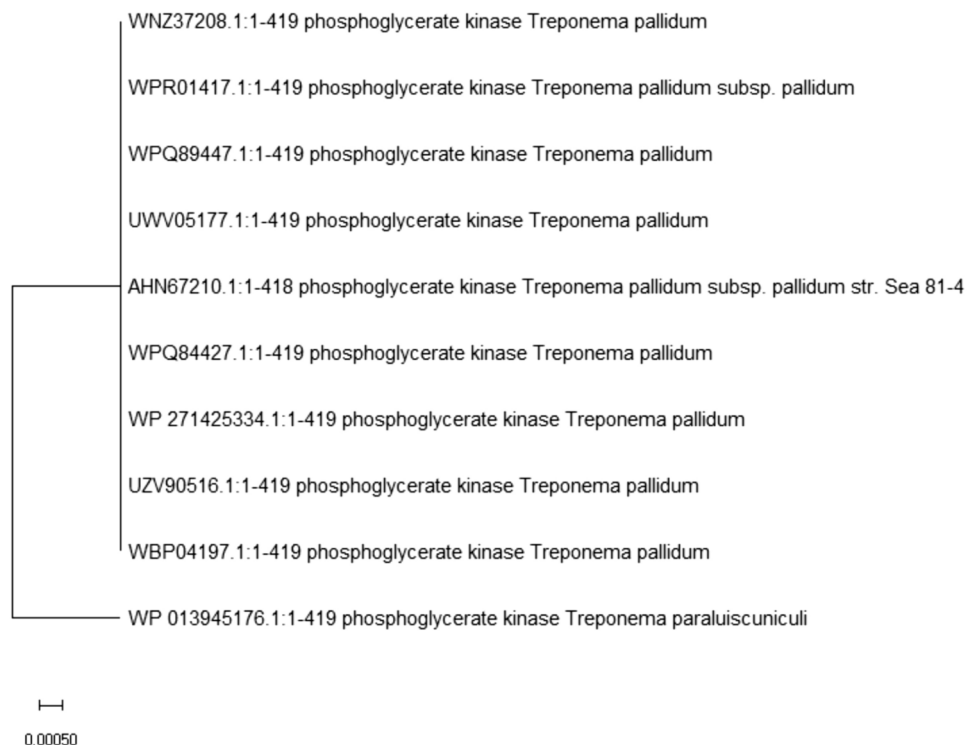
Fig. 4. Phylogenetic tree of *Phosphoglycerate Kinase (PGK)* across *Treponema pallidum* strains and closely related species through MEGA 11 software. The evolutionary relationship confirms the conservation of PGK binding site residues, supporting their reliability for ligand binding.
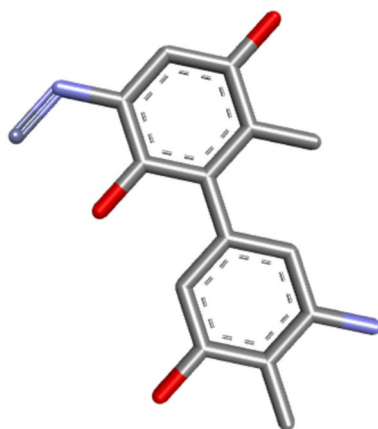
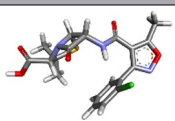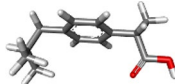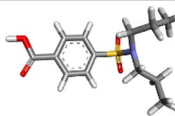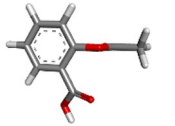**Fig. 5**. Designed Ligand by MarvinSketch online.
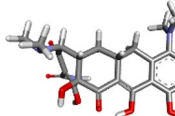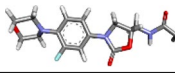
has a stronger affinity for the target protein, suggesting its potential to function more effectively. A visual representation of the docked complex is provided in Fig. 6 with docking scores through PyRx in Table 3.
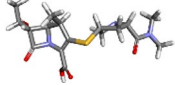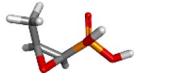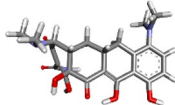
Pharmacophore modeling
The pharmacophore characterization of 1,1′-bi(cyclohexane) with the target protein is illustrated in Fig. 7. PHARMIT analysis revealed that 1,1′-bi(cyclohexane) possesses four hydrogen acceptors, four hydrogen donors, and two hydrophobic sites. This abundance of pharmacophore features indicates that 1,1′-bi(cyclohexane) is well-suited for interacting with the receptor, forming a substantial number of interactions and demonstrating strong bonding potential represented in Fig. 8.

Comparison of pharmacological profile
SwissADME webserver conducted the pharmacological analysis of both the 1,1′-bi(cyclohexane) and penicillin. The 1,1′-bi(cyclohexane) showed good solubility properties without violating Lipinski's role (Table 4).

Sr #	Inhibitors	PubChem CID	3D structure
1.	Penicillin	6098	
2.	Ibuprofen	3672	
3.	Probenecid	4911	
4.	Aspirin	2244	
5.	Moxifloxacin	152,946	
6.	Linezolid	441,401	
7.	Meropenem	441,130	
8.	Fosfomycin	446,987	
9.	Minocycline	54,675,783	
10.	Chloramphenicol	5959	

Table 2. Representation of 3D structures of various inhibitors targeting PGK in *Treponema pallidum*.
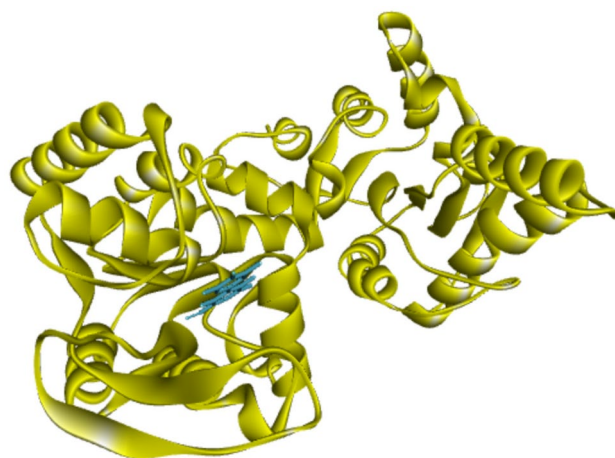

Fig. 6. Representation of designed ligand and protein *Phosphoglycerate Kinase* docked complex.

Sr #	Inhibitors	Binding affinity Kcal/mol
1.	1,1′-bi(cyclohexane)	− 6.5
2.	Penicillin	− 6.2
3.	Ibuprofen	− 5.5
4.	Probenecid	− 5.2
5.	Aspirin	− 5.2
6.	Moxifloxacin	− 6.2
7.	Linezolid	− 6.4
8.	Meropenem	− 6.2
9.	Fosfomycin	− 4.1
10.	Minocycline	− 6.3
11.	Chloramphenicol	− 5.6

Table 3. Docking scores of various inhibitors targeting *Treponema pallidum* in neurosyphilis treatment.
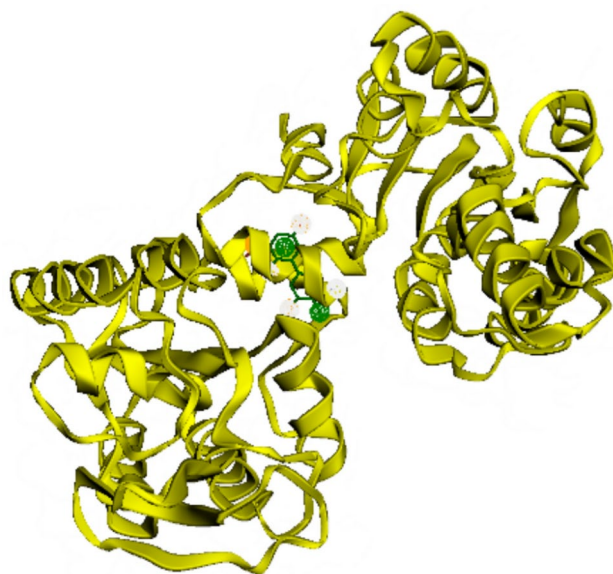
Fig. 7. Pharmacophore characterization of dock-complex by Pharmit.

Additionally, the designed ligand crossed the gastrointestinal tract with a PGP + value, suggesting that the drug candidate can pass through biological membranes easily (Fig. 9).

Comparison of toxicity profile
Protox ii predicted the toxicity profile of both the 1,1′-bi(cyclohexane) and penicillin. Penicillin showed Active respiratory toxicity with a probability of 0.96, while the 1,1′-bi(cyclohexane) represented a neutral profile. Table 5 shows the type of toxicity along with the prediction and probability of its cause.

Interaction analysis
Interaction analysis was performed, to check the interaction between the target protein and the 1,1′-bi(cyclohexane) showed the best affinity. PLIP server predicted that there are 5 hydrophobic bonds along with 3 hydrogen bonds present in the interaction Table 6 containing values and visualization of the docked complex from the PLIP server are given in Fig. 10A–C and Tables 7, and 8.

DFT analysis
Optimization of the 1,1′-bi(cyclohexane) highlighted that the compound reached a stable state with the calculated total electronic energy. The low RMS gradient reported over the optimization coverage quantifies how well it covers toward a minimum energy configuration. Figure 11 represents the optimized structure of the 1,1′-bi(cyclohexane). On the other hand, the energy gap between HOMO and LUMO plays a vital role in ligand reactivity. In the case of DFT analysis, the energy band gap became smaller, showing a higher reactivity and improved electronic interaction with other molecules, as shown in Table 9. When the HOMO and LUMO wave functions are depicted in Table 10, Figs. 12 and 13, respectively.
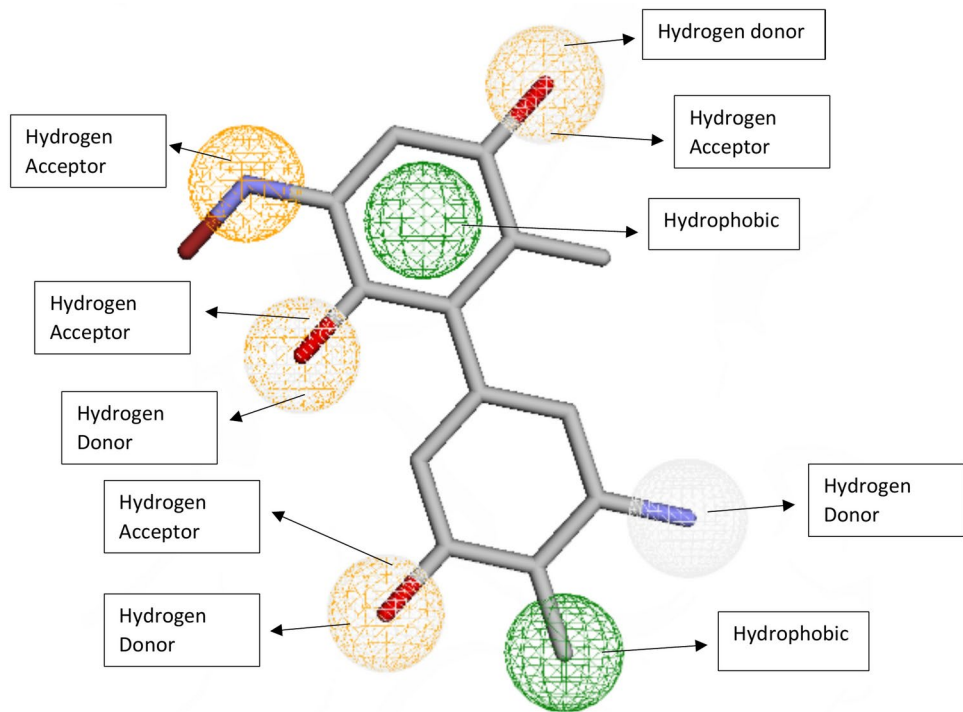
Fig. 8. The pharmacophore characterization of the designed ligand, 1,1′-bi(cyclohexane), is illustrated, with the bond-forming sites highlighted in circles. These sites represent atoms capable of interacting with the target protein, facilitating the formation of bonds that contribute to the ligand's binding efficacy and stability.

ADME analysis of 1,1′-bi(cyclohexane)		ADME analysis of Penicillin	
ADMET parameters	**Parametric values**	**ADMET parameters**	**Parametric values**
Formula	$C_{14}H_{27}N_2O_3Zn$	Formula	$C_{19}H_{18}ClN_3O_5S$
Molecular weight	336.76 g/mol	Molecular weight	435.88 g/mol
Num. of heavy atoms	20	Num. of heavy atoms	29
Fraction Csp3	1	Fraction Csp3	0.37
Num. of rotatable bonds	2	Num. of rotatable bonds	5
Num. of hydrogen bond acceptors	5	Num. of hydrogen bond acceptors	6
Num. of hydrogen bond donors	5	Num. of hydrogen bond donors	2
Molar refractivity	73.12	Molar refractivity	110.74
TPSA (topological polar surface area)	98.74 Å^2	TPSA (topological polar surface area)	138.04 Å^2
Water solubility log S (ESOL)	−1.70 (Very Soluble)	Water solubility log S (ESOL)	−4.02 (Moderately soluble)
GI absorption	High	GI absorption	High
Skin permeation (Log Kp)	−8.47 cm/s	Skin permeation (Log Kp)	−7.23 cm/s
Bioavailability score	0.55	Bioavailability score	0.56
Synthetic accessibility	4.66	Synthetic accessibility	4.61

Table 4. Comparison of Pharmacological profiles through the SwissADME server.

Molecular dynamic simulations

MD simulations were run on the *Phosphoglycerate Kinase* protein structure and Complex of target protein and 1,1′-bi(cyclohexane) ligand. The OpenMM engine and AMBER force field were utilized for protein–ligand interaction methods. For this process, the force field of ff19SB was applied. In addition, 0.15 M NaCl along with TIP3P water was incorporated into the system. Ligand topology was generated by utilizing GAFF2; then the system was equilibrated for 20,000 minimizing steps at 5000 ps. In the MD equilibration of the system, pressure and temperature values used were 1 ATM and 298 K respectively. The Apo protein and complex were then subjected to an MD simulation run for a 100 ns and 300 ns period respectively.
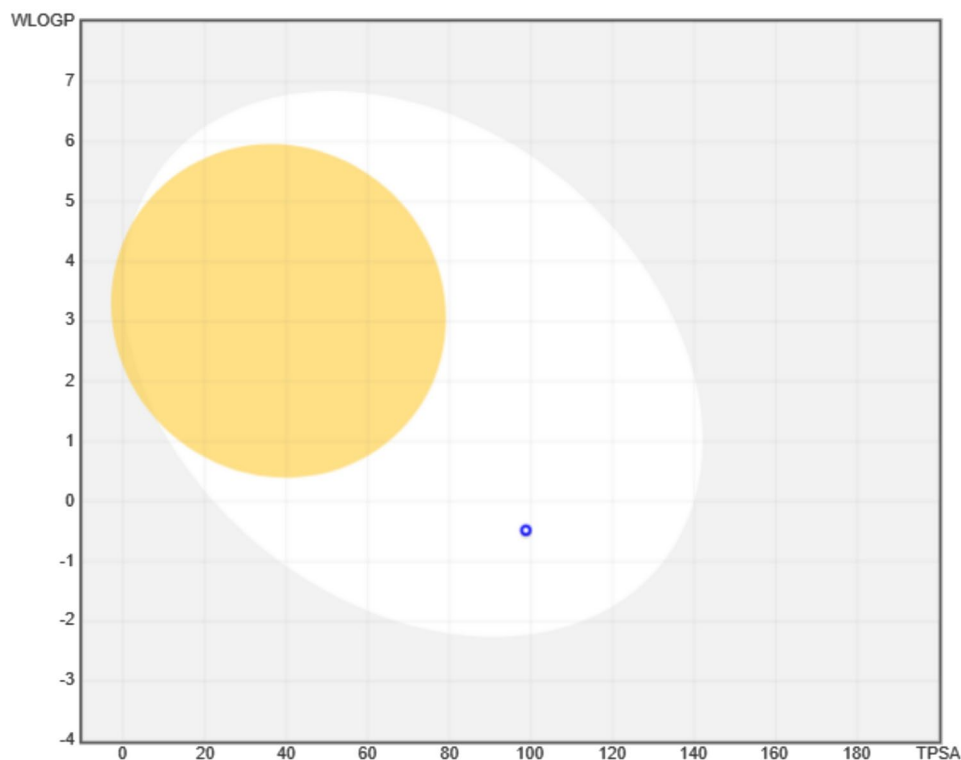
Fig. 9. The Boiled Egg diagram for 1,1′-bi(cyclohexane) illustrates the pharmacokinetic properties of the molecule. The yellow region represents compounds capable of crossing the blood–brain barrier, while the white region indicates suitability for human intestinal absorption. The analysis predicts that the designed ligand successfully crosses the gastrointestinal tract and is characterized by a PGP + value, suggesting active efflux through P-glycoprotein transport.

RMSD and RMSF of Apo protein
The RMSD analysis shows an initial rise from 1 Å to around 3 Å within 1–20 ns, indicating early structural rearrangements. Between 20 and 60 ns, the RMSD fluctuates, reflecting conformational sampling. By 60 ns, RMSD stabilizes near 4 Å, suggesting dynamic stability with moderate structural deviations. The RMSF plot highlights flexible regions, with peaks at residues 28 (ASP) and 79 (GLY), indicating localized fluctuations. The stability of the system and the retention of ligands in the binding pocket suggest strong interactions throughout the simulation. Figure 14A and B represent RMSD and RMSF graphs respectively.

Radius of gyration of Apo protein
The radius of gyration (Rg) plot shows how the molecular compactness changes over the 100 ns simulation. Initially, the Rg fluctuates around 22.6–23.4 Å, indicating minor structural rearrangements. A gradual increase in Rg is observed until ~ 50 ns, where peaks around 23.8 Å suggest a more expanded structure. However, the later phase of the simulation shows fluctuations and stabilization around 23.6 Å, indicating that the molecule retains some flexibility but remains relatively stable in a compact form (Fig. 15).

Principal component analysis of Apo protein
Principal Component Analysis (PCA) was performed on the 100 ns molecular dynamics (MD) simulation trajectory to identify dominant atomic motions and structural variations. The covariance matrix was built from the Cα backbone atoms, eliminating rotational and translational motions to focus on intrinsic atomic fluctuations. The PCA plot shows the distribution of conformational states along PC1 (− 40 to 60) and PC2 (− 40 to 30). The central cluster represents stable regions, while more dispersed regions indicate dynamic conformational changes, reflecting structural flexibility (Fig. 16).

RMSD and RMSF predictions of the complex
The predictable structure conformational changes over the simulation period of 300 ns are presented using RMSD (Root Mean Square Dot). Figure 17A represents that at the start the RMSD plot shows an initial rise from 1 to 3 Å within the first 1–20 ns, indicating early conformational adjustments. Between 20 and 60 ns, significant fluctuations suggest structural exploration. Peaks reaching 4–5.2 Å around 50–150 ns indicate transient conformational shifts. After 150 ns, the RMSD stabilizes within 3.5–4.5 Å, reflecting dynamic equilibrium. By the end of the 300 ns simulation, fluctuations decrease, with RMSD settling between 3–4 Å, suggesting a stable yet flexible structure.

Classification	Type of toxicity	Prediction (for 1,1′-bi(cyclohexane)	Probability (for 1,1′-bi(cyclohexane)	Prediction (for Penicillin)	Probability (for Penicillin)
Organ toxicity	Neurotoxicity	Inactive	0.62	Inactive	0.94
Organ toxicity	Nephrotoxicity	Inactive	0.50	Inactive	0.58
Organ toxicity	Respiratory toxicity	Inactive	0.67	Active	0.96
Organ toxicity	Cardiotoxicity	Inactive	0.53	Inactive	0.81
Toxicity endpoints	Carcinogenicity	Inactive	0.60	Inactive	0.66
Toxicity endpoints	Immunotoxicity	Inactive	0.95	Inactive	0.96
Toxicity endpoints	Cytotoxicity	Inactive	0.65	Inactive	0.67
Toxicity endpoints	Mutagenicity	Inactive	0.58	Inactive	0.68
Toxicity endpoints	Clinical toxicity	Inactive	0.62	Inactive	0.57
Toxicity endpoints	Nutritional toxicity	Inactive	0.60	Active	0.51
Toxicity endpoints	BBB-barrier	Inactive	0.61	Inactive	1.0
Toxicity endpoints	Ecotoxicity	Inactive	0.59	Inactive	0.57
Tox21-Nuclear receptor signaling pathways	Aryl hydrocarbon Receptor (AhR)	Inactive	0.91	Inactive	0.89
Tox21-Nuclear receptor signaling pathways	Androgen Receptor (AR)	Inactive	0.91	Inactive	0.96
Tox21-Nuclear receptor signaling pathways	Androgen Receptor Ligand Binding Domain (AR-LBD)	Inactive	0.89	Inactive	0.98
Tox21-Nuclear receptor signaling pathways	Aromatase	Inactive	0.93	Inactive	0.88
Tox21-Nuclear receptor signaling pathways	Estrogen Receptor Alpha (ER)	Inactive	0.81	Inactive	0.84
Tox21-Nuclear receptor signaling pathways	Estrogen Receptor Ligand Binding Domain (ER-LBD)	Inactive	0.86	Inactive	0.94
Tox21-Nuclear receptor signaling pathways	Peroxisome Proliferator-Activated Receptor Gamma (PPAR-Gamma)	Inactive	0.89	Inactive	0.95
Tox21-Stress response pathways	Nuclear factor (erythroid-derived 2)-like 2/antioxidant responsive element (nrf2/ARE)	Inactive	0.84	Inactive	0.95
Tox21-Stress response pathways	Heat shock factor response element (HSE)	Inactive	0.84	Inactive	0.95
Tox21-Stress response pathways	Mitochondrial Membrane Potential (MMP)	Inactive	0.83	Inactive	0.78
Tox21-Stress response pathways	Phosphoprotein (Tumor Suppressor) p53	Inactive	0.82	Inactive	0.86
Tox21-Stress response pathways	ATPase family AAA domain-containing protein 5 (ATAD5)	Inactive	0.89	Inactive	0.95
Molecular Initiating Events	Thyroid hormone receptor alpha (THRα)	Inactive	0.73	Inactive	0.65
Molecular Initiating Events	Thyroid hormone receptor beta (THRβ)	Inactive	0.82	Inactive	0.79
Molecular Initiating Events	Transthyretin (TTR)	Inactive	0.66	Inactive	0.68
Molecular Initiating Events	Ryanodine receptor (RYR)	Inactive	0.86	Inactive	0.78
Molecular Initiating Events	GABA receptor (GABAR)	Inactive	0.54	Inactive	0.80
Molecular Initiating Events	Glutamate N-methyl-D-aspartate receptor (NMDAR)	Inactive	0.81	Inactive	0.95
Molecular Initiating Events	alpha-amino-3-hydroxy-5-methyl-4-isoxazolepropionate receptor (AMPAR)	Inactive	0.98	Inactive	0.96
Molecular Initiating Events	Kainate receptor (Nahian et al.)	Inactive	0.99	Inactive	0.96
Molecular Initiating Events	Acetylcholinesterase (Tulloch)	Inactive	0.83	Inactive	0.92
Molecular Initiating Events	Constitutive androstane receptor (Laskowski et al.)	Inactive	0.99	Inactive	0.99
Molecular Initiating Events	Pregnane X receptor (PXR)	Inactive	0.78	Active	0.57
Molecular Initiating Events	NADH-quinone oxidoreductase (NADHOX)	Inactive	0.77	Inactive	0.93
Molecular Initiating Events	Voltage gated sodium channel (VGSC)	Inactive	0.75	Inactive	0.82
Molecular Initiating Events	Na + /I- symporter (NIS)	Inactive	0.90	Inactive	0.93
Metabolism	Cytochrome CYP1A2	Inactive	0.89	Inactive	0.99
Metabolism	Cytochrome CYP2C19	Inactive	0.86	Inactive	0.98
Metabolism	Cytochrome CYP2C9	Inactive	0.78	Inactive	0.84
Metabolism	Cytochrome CYP2D6	Inactive	0.64	Inactive	0.97
Metabolism	Cytochrome CYP3A4	Inactive	0.90	Inactive	1.0
Metabolism	Cytochrome CYP2E1	Inactive	0.99	Inactive	0.99

Table 5. Comparison of toxicity between designed ligand and penicillin through Protox ii.

Moreover, the RMSF (root mean square fluctuation) value was used to describe the structure stability of the protein and flexibility or variability in the residue at the time of a protein hit interaction. By simulations, the graph's peaks relate to the protein's fluctuation portion. The peaks on the graph on horizontal axes i.e. on residue numbers 28 (ASP) and 79 (GLY) represented in Fig. 17B showed the amplitude of the protein change over the

Index	Residues	Amino Acids	Distance (Å)	Ligand atom	Protein atom
1.	220A	ALA	3.86	3162	1714
2.	261A	LEU	3.96	3168	2003
3.	261A	LEU	3.95	3167	2000
4.	296A	PHE	3.63	3167	2261
5.	345A	VAL	3.70	3156	2631

Table 6. Representation of hydrophobic interactions between protein Phosphoglycerate Kinase (Chain A) interacting with 1,1′-bi(cyclohexane) through PLIP webserver.

specific period throughout the simulation. After this analysis, it was confirmed that systems were stable and ligands did not escape from the binding pockets demonstrating important interactions.

Radius of Gyration (rGyr) and interaction energy of complex
As the radius of gyration represents the 'stretch' of a ligand, the number is thus a ligand's principal moment of inertia. In Fig. 18, the graph represents the amount of time and the radius of gyration of a molecule throughout a 300 ns simulation with values ranging from about 24.5 Å at the start to around 23 Å between 50 and 150 ns. The observed decreasing trend with variations suggests that the molecule contracts into a more compact structure as the simulation continues. After 150 ns, the Rg begins to gradually increase, around 250 ns onwards, a more pronounced rise in Rg values is observed, reaching 25 Å at the end of the simulation, suggesting increased flexibility or partial unfolding.

In Fig. 19 The graph shows the pattern of the interaction energy obtained from molecular dynamics simulation for 300 ns having electrostatic energy (blue color), van der Waals energy (orange color), and total energy (grey color). The total interaction energy is constant within the simulation time and dominated by the van der Waals forces, whereas the electrostatic energy has a weak pattern fluctuating around a stable mean value.

Distance ligand-catalytic sites
The catalytic sites, comprising residues 169, 173, 174, 198, 202, 340, 374, 375, 376, 377, 380, 396, 397, 398, 399, 400, 401, 402, 403, 404, and 406, were selected with a cutoff distance of 6 Å for a simulation period of 300 ns. It fluctuates about a value of approximately 4 Å and has an initial transient rise to nearly 5.2 Å suggesting that the ligand remains in close contact with the residues even after the initial stabilization. Toward the end of the simulation, a slight increase in distance is observed, possibly indicating a minor. Figure 20A illustrates the distance between the ligand and the catalytic sites. Additionally, the distance between the ligand and selected residues, including 78, 84, and 85, is also represented in Fig. 20B. Initially, the distance fluctuates between 29–33 Å until 50 ns, then stabilizes around 27–29 Å between 50–150 ns, indicating stable ligand-residue interactions. After 150 ns, a gradual increase to 36–38 Å suggests conformational changes or weakening interaction.

Principle component analysis (PCA)
Principal Component Analysis (PCA) was used in molecular dynamics (MD) simulations to reduce the complexity of high-dimensional trajectory data by identifying dominant atomic motions. This method isolates principal components that capture the most significant variations in atomic configurations, enabling the interpretation of essential collective movements and key dynamic behaviors. During this analysis, a covariance matrix was constructed from the simulation trajectories of the backbone Cα-atoms over 300 ns of MD simulations, ensuring the elimination of rotational and translational motions to focus exclusively on intrinsic atomic fluctuations. In Fig. 21 The PCA plot shows the PCA of the MD simulation trajectory on PC 1 and PC2; with PC1 values ranging from about − 80 to 100, and PC2 from around − 50 to 50. The dots provide information on several conformational states or regions during the simulation; the dispersion of the dots characterizes the degree of structural flexibilities in the backbone Cα atoms. The areas in the center are clustered together, which can be interpreted as more stable regions, the regions dispersed in the plane are more dynamic areas of the protein structure.

Examination of MM/GBSA and PBSA binding-free energy
The Thermal_mmgbsa.py script from Desmond was employed in conjunction with the Molecular Mechanics Generalized Born Surface Area (MM/GBSA) method to calculate the binding free energies with and without TIP3P water. This approach evaluates the free energy of binding (ΔGbind) for docked configurations and trajectories derived from Desmond simulations. The computation of (ΔGbind) is based on the following equation:

$$\Delta G\,(bind) = \Delta G Complex - \Delta G Ligand - \Delta G Receptor$$

where ΔGComplex in MM/GBSA corresponds with the energy estimations of the optimized complex (complex), ΔGLigand, and ΔGReceptor represent the energy estimations of the optimized free ligand (ligand) and the optimized free receptor (receptor) respectively.

The MM/GBSA (Molecular Mechanics Generalized Born Surface Area) method is the most widely utilized approach for calculating binding free energy due to its high accuracy compared to conventional molecular docking scoring systems. This method has gained extensive application in bio-molecular research, including
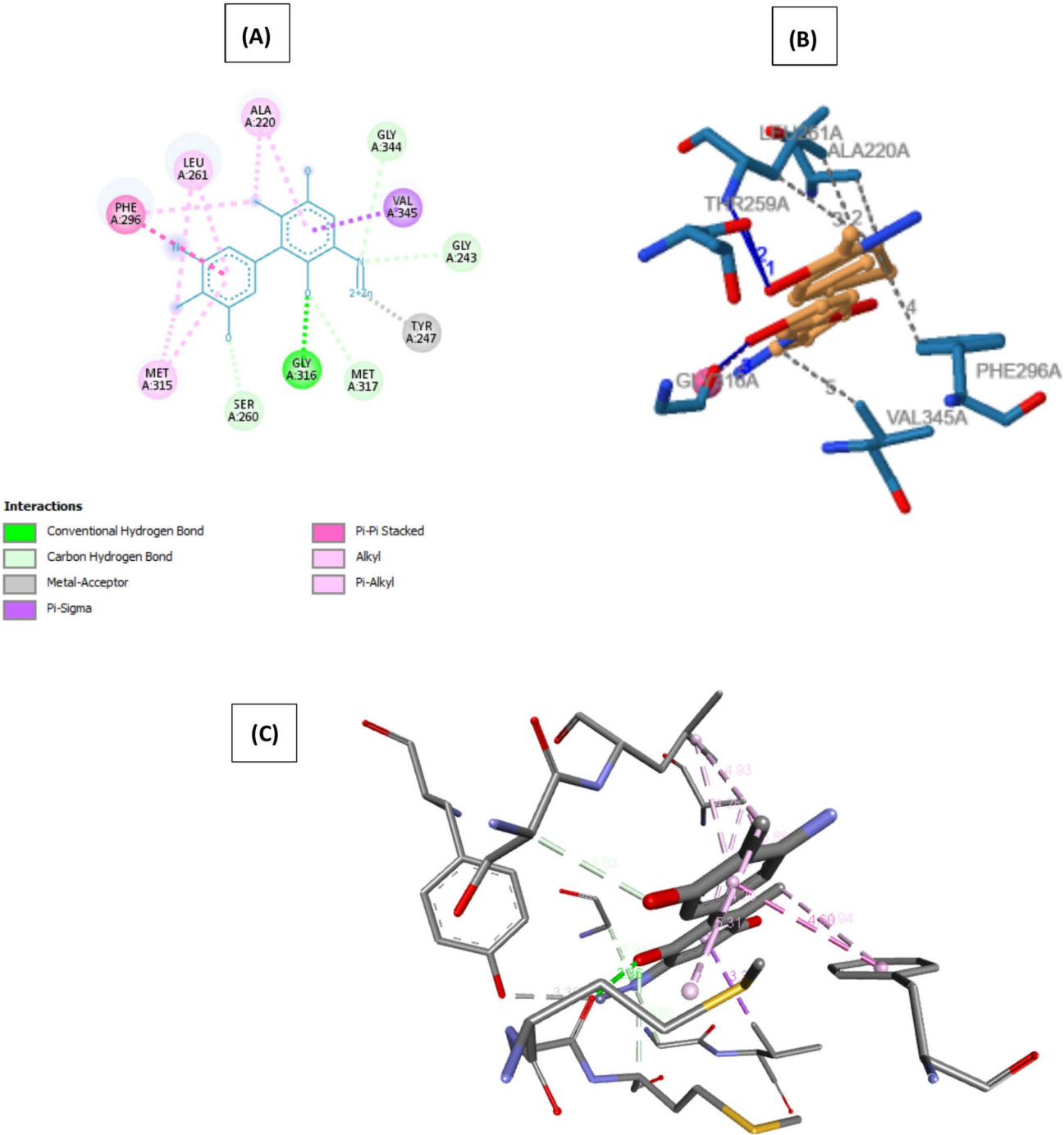
Fig. 10. (**A**) 2D interaction representation through DSV, (**B**) 3D Interaction analysis of docked complex through PLIP, (**C**) 3D interaction representation of ligand through DSV.

Index	Residues	Amino Acids	Distance H-A	Distance D-A	Donor angle	Protein donor?	Donor atom	Acceptor atom
1.	259A	THR	2.73	3.61	150.05	no	3169 (O3)	1986 (O2)
2.	261A	LEU	2.55	3.21	124.30	yes	1996 [Nam]	3169 [O3]
3.	316A	GLY	1.43	2.36	159.70	no	3161 [O3]	2409 [O2]

Table 7. Representation of hydrogen bonds between protein Phosphoglycerate Kinase (Chain A) interacting with 1,1′-bi(cyclohexane) through PLIP webserver.

Index	Residues	Amino Acids	Metal	Target	Distance (Å)	Location
1.	0Z	UNK	3160	3161	2.67	protein.mainchain

Table 8. Representation of Metal complexes containing Zn, trigonal. pyramidal (3).
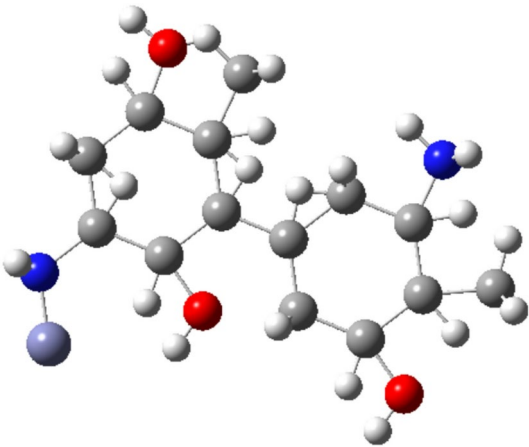
Fig. 11. Optimized structure of the designed ligand.

Final DFT	
Calculation type	**SP**
Calculation method	(UB3LYP)
Basic set	6-31G
Charge	0
Spin	Doublet
E(UB3LYP)	− 2660.58052377
Dipole moment	12.5978 Debye
Point group	C1

Table 9. Representation of DFT analysis.

Compound	ELUMO (kcal/mol)	EHOMO (kcal/mol)	Band energy gap (ΔE) (kcal/mol)
Designed Ligand	− 0.08369	− 0.09790	0.01421

Table 10. Representation of HOMO, LUMO, and Band energy gap (ΔE) (kcal/mol).

areas such as protein folding, protein–ligand binding, and protein–protein interactions. A significant advantage of MM/GBSA lies in its reduced computational demand relative to other free energy scoring methods, making it a practical choice for large-scale or complex systems.

Moreover, a critical focus in bio-molecular investigations is the quantitative determination of free energy, which underpins various molecular processes. The MM/GBSA method addresses this by incorporating the solvation-free energy changes associated with binding and the interaction energy between the ligand and the receptor. These factors enable reliable estimation of binding free energy, facilitating insights into molecular stability, interaction strength, and overall binding dynamics. Table 11 represents the MM/GBSA and MM/PBSA binding free energy calculations, both with and without TIP3P explicit water models. The van der Waals (VDWAALS) and electrostatic (EEL) interactions remain relatively consistent across methods, with slightly lower values in explicit water simulations. Solvation free energy (ΔG solv) is notably higher in MM/PBSA with TIP3P, leading to a positive total binding energy (ΔG Total), indicating instability. In contrast, MM/GBSA with TIP3P maintains a negative ΔG Total, supporting ligand binding stability. The results demonstrate that explicit water significantly influences the solvation effects and overall binding affinity, particularly in MM/PBSA calculations.
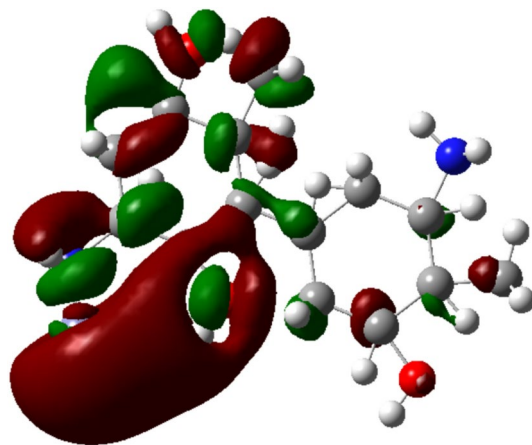
Fig. 12. Highest Occupied Molecular Orbital (HOMO) of designed ligand.
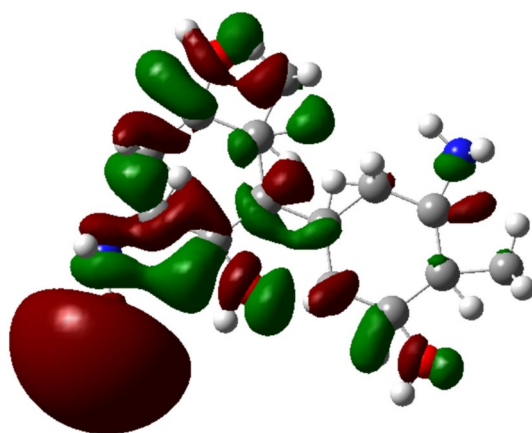

**Fig. 13**. Lowest Unoccupied Molecular Orbital (LUMO) of designed ligand.
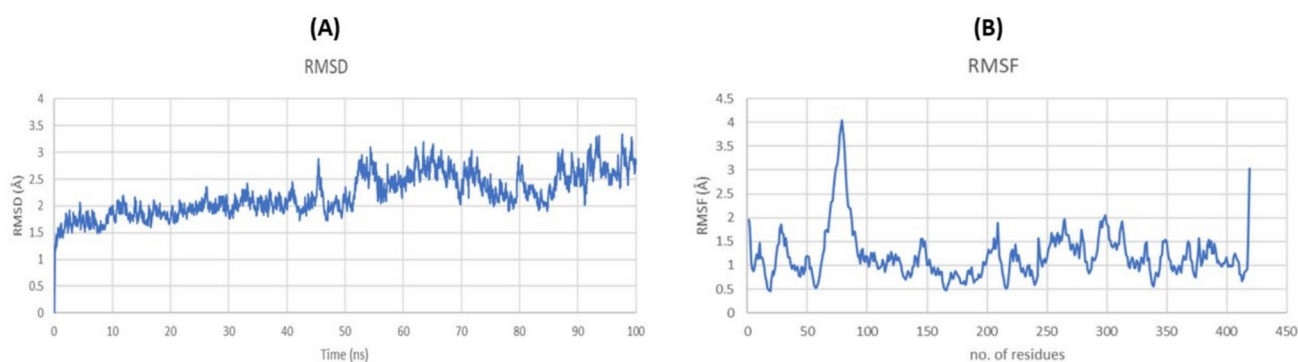
Fig. 14. (**A**) The RMSD graph illustrates the structural stability and conformational changes of the molecule over 100 ns, (**B**) The RMSF graph represents residue-wise flexibility, highlighting fluctuations in specific regions of the protein.

Discussion

Neurosyphilis disease caused by spirochaete *T. pallidum* can lead to the involvement of the meninges, brain, nerve roots, spinal cord, spinal blood vessels, and cerebral. Accordingly, the disease can appear with different and occasionally diagnostically hard appearances. They can either occur within months of the first infection or take many years to manifest, and they point to neurologic involvement in syphilis[45]. Only 30% of patients infected
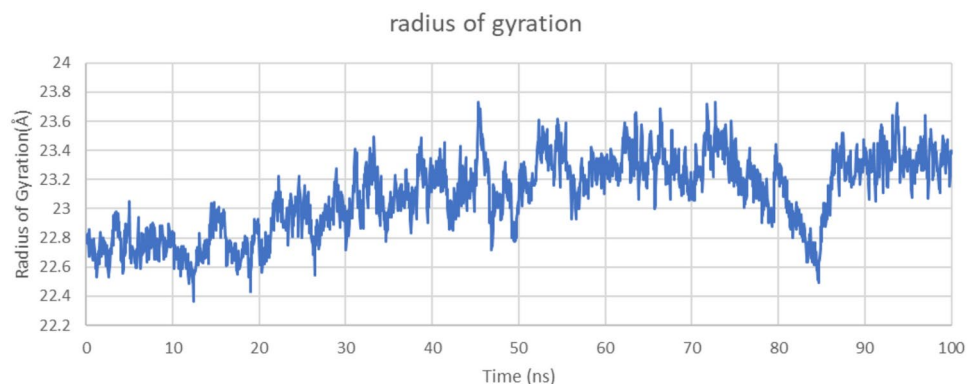
Fig. 15. Radius of gyration plot showing the structural compactness of the molecule over 100 ns, where fluctuations indicate dynamic conformational changes before achieving stability.
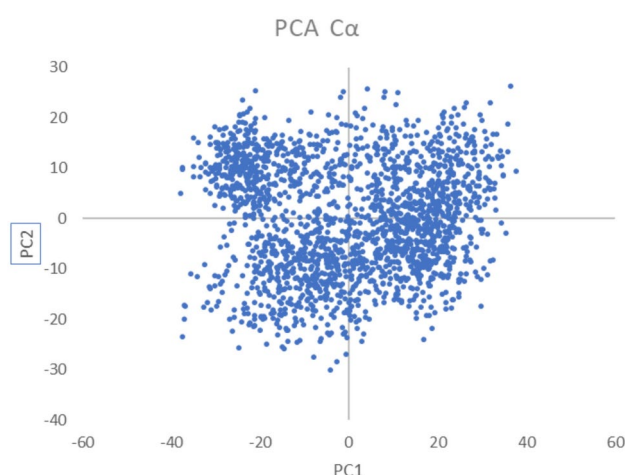

Fig. 16. Principal Component Analysis (PCA) plot of the 100 ns MD simulation, showing the conformational space explored by the system along PC1 and PC2. Clustering in the center represents stable regions, while dispersed regions indicate structural flexibility.
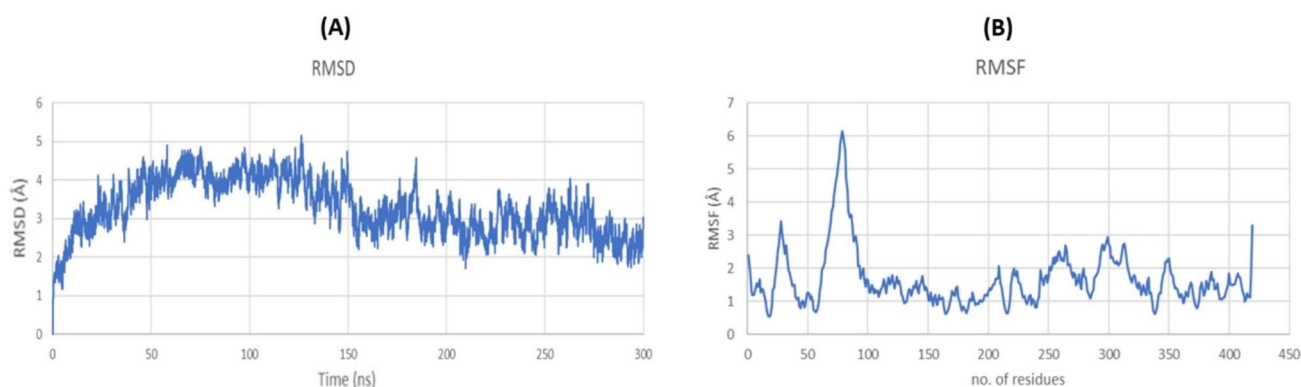

Fig. 17. (**A**) shows the RMSD value indicating total structural stability, while (**B**) shows the RMSF value showing structural fluctuations throughout the simulations.

with *T. pallidum* have cerebrospinal fluid abnormalities consistent with central nervous system penetration by the organism, yet far fewer of these progress to clinically apparent neurologic disease. The characteristics of neurosyphilis may be altered by co-existing immunosuppressive agents or diseases including HIV/AIDS. The most effective and recommended therapy is penicillin[46]. In the early 1990s, syphilis and neurosyphilis were
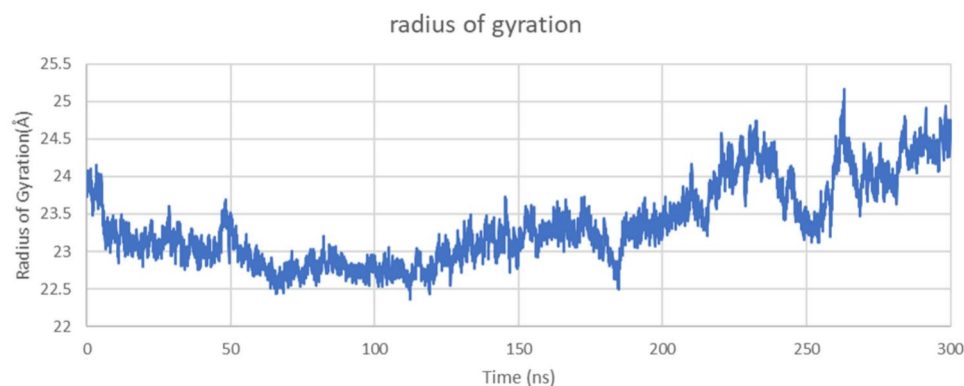
**Fig. 18**. Radius of gyration of target protein with ligand.
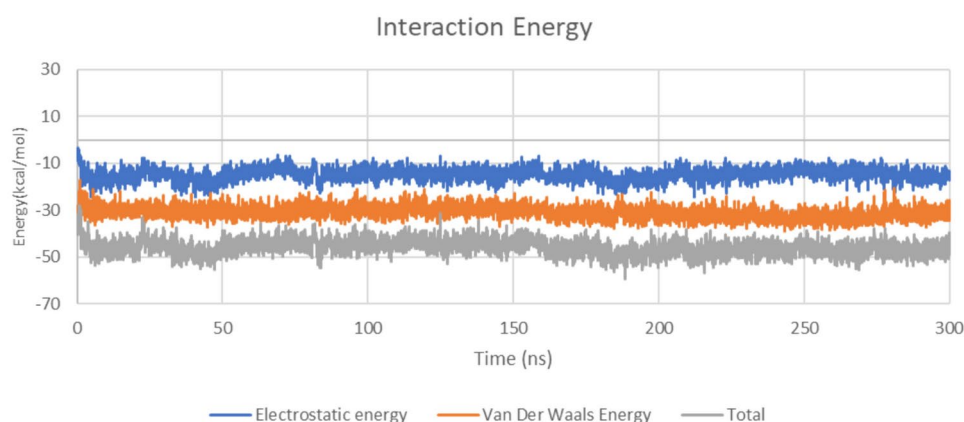
Fig. 19. Interaction energy analysis over 300 ns period of MD simulations, with van der Waals forces being the dominant contributor.
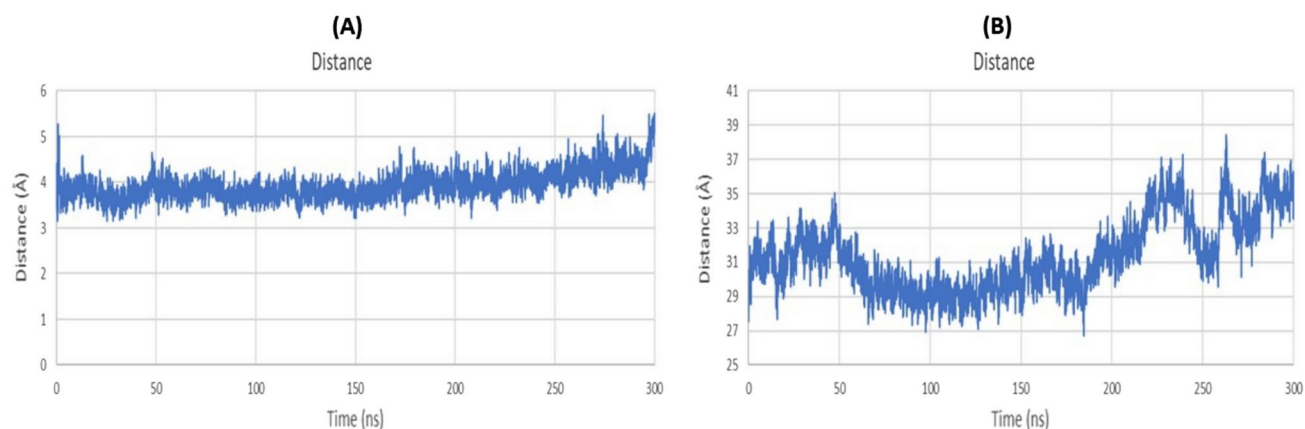
Fig. 20. (**A**) illustrates the distance between ligand-catalytic sites (**B**) Distance ligand and specific residues over a 300 ns simulation.

the major health concerns in the United States[47]. However, in a patient with distal the onset of the acquired immunodeficiency syndrome (AIDS) epidemic, there were reports of neurosyphilis in patients with HIV infection who had been appropriately treated for early syphilis, suggesting that patients with HIV may have an increased risk of neurosyphilis[48]. The diagnosis of neurosyphilis continues to pose significant challenges for clinicians. Key difficulties include the need for clear diagnostic guidelines, accurate interpretation of cerebrospinal fluid (CSF) findings, and the establishment of effective therapeutic strategies, particularly in cases requiring alternatives to
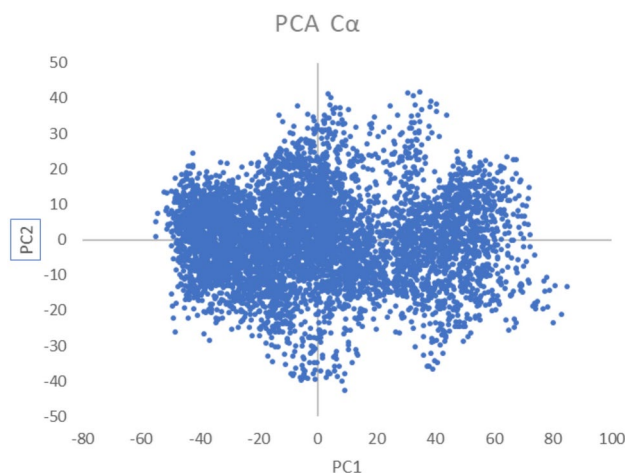
Fig. 21. Illustrates Principle component analysis during MD simulations, showing projections in PC1 and PC2 principle components for the backbone Cα atoms.

Energy Component	MMGBSA (Without TIP3P)	MMPBSA (Without TIP3P)	MMGBSA (With TIP3P)	MMPBSA (With TIP3P)
VDWAALS	− 33.1921 ± 1.5513	− 33.1921 ± 1.5513	− 28.8995 ± 4.5867	− 28.8995 ± 4.5867
EEL	− 22.9468 ± 4.0481	− 22.9468 ± 4.0481	− 15.3369 ± 1.5734	− 15.3369 ± 1.5734
EGB/EPB	32.1259 ± 2.5261	35.7266 ± 3.2704	30.2656 ± 0.6953	35.4496 ± 0.5422
ESURF/ENPOLAR	− 4.5734 ± 0.2507	− 25.0597 ± 0.8261	− 3.6358 ± 0.2859	− 21.0383 ± 2.0271
EDISPER	–	41.0934 ± 1.4274	–	34.4844 ± 2.6205
ΔG gas	− 56.1388 ± 3.5439	− 56.1388 ± 3.5439	− 44.2364 ± 3.0133	− 44.2364 ± 3.0133
ΔG solv	27.5525 ± 2.5587	51.7603 ± 3.8381	26.6298 ± 0.4094	48.8958 ± 0.0512
ΔG Total	− 28.5863 ± 3.1966	− 4.3786 ± 4.3282	− 17.6067 ± 2.6039	4.6594 ± 2.9621

Table 11. Comparison of MM/GBSA and MM/PBSA binding free energy components with and without TIP3P explicit water models. Negative ΔG Total values indicate favorable binding, whereas positive values suggest destabilization of the complex.

penicillin. Additionally, performing lumbar punctures and confirming a definitive diagnosis remain critical but complex aspects of managing this condition.[49].

Penicillin is an efficient treatment strategy and prevents late relapses[47]. Studies from 1943 to 1948 showed that early syphilis could be effectively cured with penicillin, yet 25% of secondary syphilis patients retained anti-cardiolipin antibodies, contributing researchers to search for innovative therapies. Although penicillin significantly reduced tertiary syphilis incidence, concerns remained about its ability to achieve adequate concentrations in serum and cerebrospinal fluid, leading to the assumption that a complete biological cure may be unattainable and that latent spirochetes might persist post-treatment[48]. An obvious outpatient option is intramuscular benzathine penicillin with oral probenecid. Newer agents, which freely cross the CSF, like ceftriaxone and azithromycin have not yet been properly evaluated for neurosyphilis. Syphilis increases the risk of HIV transmission and vice versa therefore, patients diagnosed with syphilis should be offered for HIV testing[50].

Zinc is present in the CNS, contributing as the second most important metal in performing physiological brain functions[51]. It promotes neurogenesis, antioxidant effect, immune system responses, activates enzymes present in neural metabolism, and regulates gene expression. Also, zinc plays an important role in synaptic activity, and neuronal plasticity acting as an efficient neuroprotective agent[52]. Moreover, nitrogen-containing compounds also act as important biologically active neuroprotective agents[53]. Also, aromatic rings contain both σ- and π-electrons causing staking (dispersed) interactions, therefore, contributing towards the stability of the structure[54]. Additionally, hydroxyl groups (-OH) are utilized, which enhance stability by forming dangling bonds and forming hydrogen bonding by interacting with other molecules, increasing the structure's overall stability[55].

In this study, de novo ligand-based drug designing was performed for building a new lead compound using ligand sketching and pharmacophore modeling techniques. Marvin Sketch online webserver was used to design a ligand based on the structural characteristics of identified neuroprotective compounds. Structural stability can be significantly enhanced by positioning two aromatic rings adjacent and introducing a zinc (Zn) element connected to NH in the first ring via a single bond. Additionally, the incorporation of two hydroxyl groups at carbon positions 2 and 5 on the same ring, and the addition of 1 hydroxyl group, 1 NH_2, and 1 CH_3 on the second ring via a single bond, has the potential to improve the stability, binding energy, and solubility of

19

the resultant ligand. This approach shows promise for advancing neuroprotective research and may lead to significant advancements in the field[56–58].

The molecular docking analysis of the ligand 1,1′-bi(cyclohexane), with Phosphoglycerate kinase, indicates a strong binding energy of −116.68 kcal/mol, alongside favorable pharmacophore characteristics and a neutral toxicity profile in comparison to the penicillin antibiotic, suggesting the efficacy of the designed ligand. Furthermore, the pharmacological profile is enhanced by a solubility value of −1.70, indicating greater aqueous solubility relative to penicillin. Interaction analysis conducted via the PLIP server reveals the presence of five hydrophobic interactions and three hydrogen bonds within the docked complex. PLIP binding interaction analysis reveals that Zn in the designed ligand interacts with the PGK mainchain at a 2.67 Å distance, forming a trigonal pyramidal metal complex. This interaction enhances binding affinity and therapeutic efficacy, stabilizing the ligand–protein complex for improved targeting of *T. pallidum*. Afterwards, the Density functional theory method was used to optimize the designed ligand, highlighting that the compound comes to a stable state. The Band energy gap (ΔE) value between the HOMO and LUMO for the ligand was predicted to be 0.01421 kcal/mol, less band gap represents the compound`s improved stability and electronic interaction with other molecules.

The approach of designed ligands would improve the therapeutic coverage and risk of resistance development. Key to this process are density functional theory (DFT) calculations that give an understanding of the electronic properties and stability of the 1,1′-bi(cyclohexane), as well as pharmacophore modeling which identifies critical features for biological activity. Together, these methodologies support improving ligand binding that will help develop specific therapeutic agents for neurosyphilis. Future studies should focus on developing ligands with targeted drug delivery systems using nanotechnology which could be administered in an exact manner leading to reducing systemic exposure and enhanced therapeutic efficacy, specifically within the central nervous system.

Conclusion

The study demonstrates an efficient strategy for the computational drug design targeting the enzyme phosphoglycerate kinase in *T. pallidum,* for treating neurosyphilis disease. Incorporating Neuroprotectant elements for designing required ligands with enhanced binding energy and reduced toxicity, proved a safe and efficient therapy against neurosyphilis disease. The successful identification of lead compounds opens new possibilities for therapeutic intervention in neurosyphilis and highlights the importance of innovative drug design approaches in treating complex infectious diseases.

Limitations and future prospective

Computational drug design may lack the ability to reflect complex biological systems and experimental studies must be required to confirm the drug′s binding affinity, interactions, effectiveness, and safety profile. Also, advanced simulations and optimization techniques could increase ligand specificity and minimization of side effects, therefore, paving the way towards new molecular-derived neuroprotective therapies for the treatment of neurosyphilis and affiliated neurodegenerative diseases. However, Future studies must focus on *in-vitro* and *in-vivo* confirmation of such compounds to assess the therapeutic potential and their further usage at clinical sites.

Data availability

All the data generated in this research work has been included in this manuscript.

References

1. Gonzalez, H., Koralnik, I. J., & Marra, C. M. *Neurosyphilis.* Paper presented at the Seminars in neurology. (2019).
2. Rotman, L. et al. Risk of neurosyphilis in HIV-infected persons with syphilis lacking signs or symptoms of central nervous system infection. *HIV Med.* **20**(1), 27–32 (2019).
3. Howard, R., Benjamin, L., De Saram, S., Houlihan, C. & Manji, H. Infection in the nervous system neurology: A queen square textbook. *Sci. World* **14**(14), 21–30 (2024).
4. Newman, L. et al. Global estimates of the prevalence and incidence of four curable sexually transmitted infections in 2012 based on systematic review and global reporting. *PloS one* **10**(12), e0143304 (2015).
5. De Voux, A., Kidd, S. & Torrone, E. A. Reported cases of neurosyphilis among early syphilis cases—United States, 2009 to 2015. *Sex. Trans. Dis.* **45**(1), 39–41 (2018).
6. Tian, T.-T. et al. Spatio-temporal analysis of incidence rate of syphilis in China. *J. Shanghai Jiaotong Univ. (Medical Science)* **41**(5), 648 (2021).
7. Crane-Kramer, G. M. M. The paleoepidemiological examination of treponemal infection and leprosy in medieval populations from northern Europe. *Unpublished doctoral dissertation). University of Calgary, Calgary, Canada.* (2001).
8. Bowater, L. The Microbiologists. *The Microbes Fight Back: Antibiotic Resistance*, 44. (2016).
9. Vanhaecke, C. et al. Clinical and biological characteristics of 40 patients with neurosyphilis and evaluation of Treponema pallidum nested polymerase chain reaction in cerebrospinal fluid samples. *Clin. Infect. Dis.* **63**(9), 1180–1186 (2016).
10. Šmajs, D., Norris, S. J. & Weinstock, G. M. J. I. Genetic diversity in Treponema pallidum: Implications for pathogenesis, evolution and molecular diagnostics of syphilis and yaws. *Infect. Genet. Evol.* **12**(2), 191–202 (2012).
11. Radolf, J. D. et al. Treponema pallidum, the syphilis spirochete: Making a living as a stealth pathogen. *Nat. Rev. Microbiol.* **14**(12), 744–759 (2016).
12. Cordwell, S. J. Microbial genomes and "missing" enzymes: Redefining biochemical pathways. *Archiv. Microbiol.* **172**, 269–279 (1999).
13. Serimbetov, Z. The structure and dynamics of phosphoglycerate kinase along its catalytic cycle: The University of Manchester (United Kingdom). (2018).
14. Milanes, J. E. et al. Enolase inhibitors as therapeutic leads for Naegleria fowleri infection. *PLoS Pathog.* **20**(8), e1012412 (2024).
15. Supuran, C. T. J. N. Carbonic anhydrases: Novel therapeutic applications for inhibitors and activators. *Nat. Rev. Drug Discov.* **7**(2), 168–181 (2008).

16. Bhardwaj, V., Singh, R., Singh, P., Purohit, R. & Kumar, S. Elimination of bitter-off taste of stevioside through structure modification and computational interventions. *J. Theor. Biol.* **486**, 110094. https://doi.org/10.1016/j.jtbi.2019.110094 (2020).
17. Singh, R., Bhardwaj, V. K. & Purohit, R. Inhibition of nonstructural protein 15 of SARS-CoV-2 by golden spice: A computational insight. *Cell Biochem. Funct.* **40**(8), 926–934. https://doi.org/10.1002/cbf.3753 (2022).
18. Singh, R., Bhardwaj, V. K., Sharma, J., Das, P. & Purohit, R. Identification of selective cyclin-dependent kinase 2 inhibitor from the library of pyrrolone-fused benzosuberene compounds: An in silico exploration. *J. Biomol. Struct. Dyn.* **40**(17), 7693–7701. https://doi.org/10.1080/07391102.2021.1900918 (2022).
19. Roney, M. & Aluwi, M. F. F. M. The importance of in-silico studies in drug discovery. *Intell. Pharm.* **2**(4), 578–579 (2024).
20. Varadi, M. et al. AlphaFold Protein Structure Database: Massively expanding the structural coverage of protein-sequence space with high-accuracy models. *Nucleic Acids Res.* **50**(D1), D439–D444 (2021).
21. Varadi, M. et al. AlphaFold protein structure database in 2024: Providing structure coverage for over 214 million protein sequences. *Nucleic Acids Res.* **52**(D1), D368–D375 (2024).
22. Laskowski, R., MacArthur, M., & Thornton, J. PROCHECK: validation of protein-structure coordinates. (2006).
23. Patgiri, P., Goyary, B., Roy, M. K., Swargiary, A., Brahma, N. R., & Brahma, B. (2024). Mutational study of voltage-gated sodium channel in permethrin resistance in mosquitoes: An in silico study. *Int. J. Pharm. Investig., 14*(3).
24. Jendele, L., Krivak, R., Skoda, P., Novotny, M. & Hoksza, D. J. N. PrankWeb: A web server for ligand binding site prediction and visualization. *Sci. World* **47**(W1), W345–W349 (2019).
25. Rahman, A. et al. Research article targeting essential hypothetical proteins of pseudomonas aeruginosa PAO1 for mining of novel therapeutics: an in silico approach. *BioMed Res. Int.* **2023**(1), 1787485 (2023).
26. Kumar, S., Stecher, G., Li, M., Knyaz, C. & Tamura, K. J. M. MEGA X: Molecular evolutionary genetics analysis across computing platforms. *Mol. Biol. Evol.* **35**(6), 1547–1549 (2018).
27. Kaushik, M. J. M. J. A review of innovative chemical drawing and spectra prediction computer software. *Mediterranean J. Chem.* **3**(1), 759–766 (2014).
28. Lestari, K., Sitorus, T., Instiaty, I., Megantara, S. & Levita, J. Molecular docking of quinine, chloroquine and hydroxychloroquine to angiotensin converting enzyme 2 (ACE2) receptor for discovering new potential COVID-19 antidote. *J. Adv. Pharm. Educ. Res.* **10**(2–2020), 1–4 (2020).
29. Burger, M. C. ChemDoodle Web Components: HTML5 toolkit for chemical graphics, interfaces, and informatics. *J. Cheminform.* **7**, 1–7 (2015).
30. Kim, S. et al. PubChem substance and compound databases. *Nucleic Acids Res.* **44**(D1), D1202–D1213 (2016).
31. Dallakyan, S., Olson, A. J. J. C. b. m., & Protocols. Small-molecule library screening by docking with PyRx. 243–250. (2015).
32. Salentin, S., Schreiber, S., Haupt, V. J., Adasme, M. F. & Schroeder, M. J. N. PLIP: Fully automated protein–ligand interaction profiler. *Nucleic Acids Res.* **43**(W1), W443–W447 (2015).
33. Studio, D. J. A. (2008). Discovery studio. *420*.
34. Paul, P. et al. Investigating the potent TOPO IIα inhibitors in breast cancer through the study of computational drug discovery research approaches. *Mol. Divers.* **29**(1), 655–670 (2024).
35. Sunseri, J. & Koes, D. R. J. N. Pharmit: Interactive exploration of chemical space. *Nucleic Acids Res.* **44**(W1), W442–W448 (2016).
36. Naveed, M. et al. Assessment of Melia azedarach plant extracts activity against hypothetical protein of mycobacterium tuberculosis via GC-MS analysis and in-silico approaches. *J. Comput. Biophys. Chem* **23**(3), 299–320 (2024).
37. Daina, A., Michielin, O. & Zoete, V. J. S. SwissADME: A free web tool to evaluate pharmacokinetics, drug-likeness, and medicinal chemistry friendliness of small molecules. *Sci. Rep.* **7**(1), 42717 (2017).
38. Banerjee, P., Eckert, A. O., Schrey, A. K. & Preissner, R. J. N. ProTox-II: A web server for the prediction of toxicity of chemicals. *Nucleic Acids Res.* **46**(W1), W257–W263 (2018).
39. Joshi, B. D., Thakur, G. & Chaudhary, M. K. J. S. W. Molecular structure, homo-lumo and vibrational analysis of ergoline by density functional theory. *Sci. World* **14**(14), 21–30 (2021).
40. Obu, Q. S. et al. Synthesis, spectra (FT-IR, NMR) investigations, DFT study, in silico ADMET and Molecular docking analysis of 2-amino-4-(4-aminophenyl) thiophene-3-carbonitrile as a potential anti-tubercular agent. *J. Mol. Struct.* **1244**, 130880 (2021).
41. Salomon-Ferrer, R., Case, D. A. & Walker, R. C. J. W. I. R. C. M. S. An overview of the Amber biomolecular simulation package. *Wiley Interdiscip. Rev.: Comput. Mol. Sci.* **3**(2), 198–210 (2013).
42. Henderson, J. A. et al. A guide to the continuous constant pH molecular dynamics methods in Amber and CHARMM. *Liv. J. Comput. Mol. Sci.* **4**(1), 1563 (2022).
43. Wang, E. et al. End-point binding free energy calculation with MM/PBSA and MM/GBSA: Strategies and applications in drug design. *Chem. Rev.* **119**(16), 9478–9508 (2019).
44. Lagarias, P. et al. Insights to the binding of a selective adenosine A3 receptor antagonist using molecular dynamic simulations, MM-PBSA and MM-GBSA free energy calculations, and mutagenesis. *J. Chem. Inf. Model.* **59**(12), 5183–5197 (2019).
45. Berger, J. R. & Dean, D. Neurosyphilis. *Handbook Clin. Neurol.* **121**, 1461–1472 (2014).
46. Ha, T., Tadi, P., Leslie, S., & Dubensky, L. Neurosyphilis. *StatPearls*. (2024).
47. Patterson, D., Vilensky, J. A., Robertson, W. M. & Berger, J. Treatment and diagnostic accuracy of neurosyphilis at Boston city hospital's neurological unit, 1930–1979. *J. Neurol. Sci.* **314**(1–2), 1–4 (2012).
48. Musher, D. M. Syphilis, neurosyphilis, penicillin, and AIDS. *J. Infect. Dis.* **163**(6), 1201–1206 (1991).
49. O'Donnell, J. A. & Emery, C. L. Neurosyphilis: A current review. *Curr. Infec. Dis. Rep.* **7**(4), 277–284 (2005).
50. Jay, C. A. Treatment of neurosyphilis. *Curr. Treat. Options Neurol.* **8**(3), 185–192 (2006).
51. Singla, N. & Dhawan, D. Zinc, a neuroprotective agent against aluminum-induced oxidative DNA injury. *Mol. Neurobiol.* **48**, 1–12 (2013).
52. Li, Z., Liu, Y., Wei, R., Yong, V. W. & Xue, M. The important role of zinc in neurological diseases. *Biomolecules* **13**(1), 28 (2022).
53. Das, S. et al. Recent advancement of pyrazole scaffold based neuroprotective agents: A review. *CNS & Neurol. Disord.-Drug Targets (Formerly Current Drug Targets-CNS & Neurological Disorders)* **21**(10), 940–951 (2022).
54. Riley, K. E. & Hobza, P. On the importance and origin of aromatic interactions in chemistry and biodisciplines. *Acc. Chem. Res.* **46**(4), 927–936 (2013).
55. Fileti, E. E., Rivelino, R., de Brito Mota, F. & Malaspina, T. Effects of hydroxyl group distribution on the reactivity, stability and optical properties of fullerenols. *Nanotechnology* **19**(36), 365703 (2008).
56. Nahian, M. et al. In silico design of an epitope-based vaccine against PspC in Streptococcus pneumoniae using reverse vaccinology. *J. Genet. Eng. Biotechnol.* **21**(1), 166 (2023).
57. Tulloch, R. The genomics of viral respiratory disease in Australia: Understanding the spread evolution and pathogenesis of non-influenza respiratory viruses. (2023).
58. Yan, Y., Zhang, D., Zhou, P., Li, B. & Huang, S.-Y.J.N. HDOCK: A web server for protein–protein and protein–DNA/RNA docking based on a hybrid strategy. *Nucleic Acids Res.* **45**(W1), W365–W373 (2017).

Acknowledgements

Author contributions

Conceptualization, M.N.; methodology, S.I.; software, M.A.; validation, M.N.M.; formal analysis, A.A.K..; investigation, M.N.M., resources, T.A..; data curation, R.A.E.H.M. and M.S.A..; writing—original draft preparation, M.A..; writing—review and editing, R.A.E.H.M., M.S.A., F.A.Al-J. and D.F.; visualization, S.I.; supervision, M.N. and T.A..; project administration, T.A.

Declarations

Competing interests

The authors declare no competing interests.

Additional information

Correspondence and requests for materials should be addressed to M.N. or T.A.

Reprints and permissions information is available at www.nature.com/reprints.

Publisher's note Springer Nature remains neutral with regard to jurisdictional claims in published maps and institutional affiliations.